

Supplemental data

Mutations in *FOXE3* Cause Familial Thoracic Aortic Aneurysms and Dissections

S.Q. Kuang¹, O. Medina-Martinez², D.C. Guo¹, L. Gong¹, E.S. Regalado¹, C.L. Reynolds³, C. Boileau⁴, G. Jondeau⁵, S.K. Prakash¹, C.S. Kwartler¹, L.Y. Zhu¹, A.M. Peters¹, X.Y. Duan¹, GenTAC Investigators, National Heart, Lung, and Blood Institute Go Exome Sequencing Project; M.J. Bamshad⁶, J. Shendure⁶, D.A. Nickerson⁶, R.L. Santos-Cortez⁷, X.R. Dong⁸, S.M. Leal⁷, M.W. Majesky⁸, E.C. Swindell⁹, M. Jamrich², D. M. Milewicz¹

The GenTAC investigators

Johns Hopkins University

Williams Ravekes, M.D.

Harry C. Dietz, M.D., Ph.D.

Jennifer Habashi, M.D.

University of Texas - Houston

Dianna M. Milewicz, M.D. Ph.D.

Siddharth K. Prakash, M.D., Ph.D

Baylor College of Medicine

Scott A. LeMaire. M.D.

Shaine A. Morris, M.D.

Oregon Health & Science University

Cheryl L Maslen, Ph.D.

Howard K. Song, M.D., Ph.D

G. Michael Silberbach, M.D.

Kathryn W. Holmes, M.D.

University of Pennsylvania

Reed E. Pyeritz, M.D., Ph.D.

Joseph E. Bavaria M.D.

Karianna Milewski, M.D., Ph.D.

Weill Medical College of Cornell University

Richard B. Devereux, M.D., Ph.D.

Jonathan W. Weinsaft, M.D.

Mary J. Roman, M.D.

The Queen's Medical Center

Ralph Shohet, M.D.

MedStar Health Research Institute

Federico M. Asch, M.D.

University of Michigan

Kim A. Eagle, M.D.

National Heart, Lung, and Blood Institute

H. Eser Tolunay, Ph.D.

Patrice Desvigne-Nickens, M.D.

National Institute of Arthritis, Musculoskeletal and Skin Diseases

Hung Tseng, PhD

RTI International

Barbara L. Kroner, Ph.D.

Supplemental Figure Legends

Supplemental Figure 1

Foxe3^{-/-} mice have reduced medial cell density and total number of medial cells in ascending aorta and aortic arch. No aortic enlargement or additional pathologic changes in *Foxe3*^{-/-} ascending aortas compared with wild-type (WT) aortas. (A) Representative cross sections of ascending aorta (ASC), aortic arch and descending aorta (proximal thoracic descending aorta, DES-1 and distal descending thoracic aorta, DES-2) from WT and *Foxe3*^{-/-} mice at age of 4 weeks with H&E staining. (B) Bar-graph shows the mean diameter of the ascending aortic lumen measured by echocardiograph from WT (n=13) and *Foxe3*^{-/-} mice (n=14) at 3 months of age (NS, not statistically significant). (C) Representative cross sections of ascending aorta (ASC) and aortic arch from WT and *Foxe3*^{-/-} mice at age of 6 months with H&E staining and Verhoeff-van Gieson (VVG, for elastin) staining. The right side bar-graphs show that the aortic wall thickness or the number of elastic lamellae are not different between *Foxe3*^{-/-} and WT genotypes at P1, 4 weeks and 6 months. The bottom bar-graphs show the medial cell density (mean number of medial cells divided by total medial area) and total medial cells per cross section, of the ascending aorta, aortic arch or descending aorta at 6 months of age. The medial cell density and total medial cells are significantly lower in the ascending aorta and aortic arch in *Foxe3*^{-/-} mice than WT mice; there is no statistical significant difference in the descending aorta (n = 5 per group; * $P < 0.05$, *t*-test, NS, not statistical significant). All scale bars corresponds to 100 μm , all error bars indicate s.d. from average.

Supplemental Figure 2

1.6 year-old *Foxe3*^{-/-} mice have decreased medial cell density in the ascending aorta but lack additional aortic pathology when compared with wild-type (WT) mice of the same age. Ascending aortic cross sections were stained by H&E and Verhoeff-van Gieson (VVG, for elastin) staining. Right side bar-graphs show the quantification of aortic medial cell density (mean medial cell numbers divided by medial area (mm²), the number of elastin lamellae, total medial area and aortic wall thickness. Except for the reduced medial cell density in the ascending aorta of the mutant mice, there was no other apparent histological abnormality or enlargement in *Foxe3*^{-/-} mice when compared with WT mice of the same age (n = 5 per group; NS, not statistically significant, * *P*<0.05, *t*-test). All scale bars corresponds to 100 μm, all error bars indicate s.d. from average.

Supplemental Figure 3

Ascending aortic dilatation, intramural hemorrhage or rupture in *Foxe3*^{-/-} mice following transverse aortic constriction (TAC). **(A)** Representative gross architecture of aortic aneurysm in the ascending aortas in *Foxe3*^{-/-} mice after TAC. Whole thoracic aorta were carefully isolated and examined under a dissecting microscope. *Foxe3*^{-/-} mice challenged with TAC causing aortic hematoma in the proximal ascending aorta. The H&E image of the aortic wall with blood in it shows inflammatory cells, blood, and connective tissue but the aortic medial layer is not present. **(B)** Echocardiography analysis shows increased dilation of the aorta with TAC in *Foxe3*^{-/-} mice. **(C)** Representative cross sections of mouse ascending aorta from WT and *Foxe3*^{-/-} mice with TAC for 2 weeks. Cross sections were stained by Movat pentachrome (for elastin and proteoglycan) and VVG elastin staining. All scale bars corresponds to 100 μm.

Supplemental Figure 4

Significantly down-regulation of inflammatory and smooth muscle cell (SMC) differentiation marker gene expression, along with decreased macrophage infiltration in *Foxe3^{-/-}* ascending aorta two weeks after TAC. (A) Q-PCR analysis of expression levels of expression of *Mmp2*, *Mmp9* and *Il6* in ascending aortic tissues from wild-type (WT) and *Foxe3^{-/-}* mice two weeks after TAC. Gene expression levels were normalized to *Gapdh* (n = 5 per group; ** $P < 0.01$, *t*-test). (B) Immunofluorescent staining for macrophage marker MOMA-2. Transverse cryosections (7 μ m) of ascending aorta were prepared from WT and *Foxe3^{-/-}* mice two weeks after TAC. Nuclei were stained with DAPI (blue); Elastic lamellae of the media are green (autofluorescence); Positive staining is red (Texas red-conjugated secondary antibody). Below is the bar-graph with quantification of the immunostaining for macrophage marker MAC2, showing the percentage of anti-MAC2 positive cells in ascending aorta from WT and *Foxe3^{-/-}* mice two weeks after TAC (n = 5 per group; * $P < 0.05$, *t*-test). c, Q-PCR analysis of SMC-specific gene (*Acta2*, *Myh11* and *Cnn1*) expression in ascending aortic tissues from WT and *Foxe3^{-/-}* mice. Gene expression levels were normalized to *Gapdh* (n = 5 per group; ** $P < 0.01$, *t*-test). All scale bars corresponds to 100 μ m, all error bars indicate s.d. from average.

Supplemental Figure 5

Representative cross sections of ascending aorta from *p53^{-/-}* and WT mice at age of 12 weeks. Cross sections of the ascending aorta were stained by H&E, VVG-elasticin, Movat and Terminal deoxynucleotidyl transferase dUTP nick end labeling (TUNEL) staining. Bar-graphs on the right show the aortic total number of medial cells per cross section, medial cell density (mean medial cell numbers divided by medial area (mm^2), total medial area (mm^2), number of elastin lamellae

and the percentage of medial apoptotic cells (n = 5 per group; NS, not statistically significant, *t*-test). All scale bars corresponds to 100 μ m, all error bars indicate s.d. from average. No aortic histological and pathologic changes were identified in *p53*^{-/-} ascending aortas compared with wild-type (WT) aortas.

Supplemental Figure 6

Foxe3 mutants lens phenotype is not rescued with deficiency of p53. **(A-C)** Immunostaining using anti-phospho-histone H3 staining (PH3) for proliferative cells of sections of embryonic E16.5 lens. **(A)** The double heterozygote *Foxe3*^{+/-}/*p53*^{+/-} mice show the normal morphology of Wild-type (WT) lenses with proliferative cells (black arrow) restricted to the anterior epithelial cells **(B)** *Foxe3*^{-/-} lenses are smaller and vacuolated and show reduced proliferation activity in the anterior epithelium. **(C)** *Foxe3*^{-/-}/*p53*^{-/-} double mutant mice have the same characteristic microphakia and reduced proliferation as the *Foxe3*^{-/-} lens. **(D-I)** H&E staining of postnatal eyes (p21). **(D)** WT. **(E)** Double heterozygotes *Foxe3*^{+/-}/*p53*^{+/-} and **(F)** *p53*^{-/-} showing the normal lens morphology. **(G) and (H)** *Foxe3*^{-/-}/*p53*^{+/-} lenses are smaller and are vacuolated with absence of the anterior segment. **(I)** *Foxe3*^{-/-}/*p53*^{-/-} show a very similar lens phenotype consisting of a vacuolated small lens but the retina shows the abnormal folding previously reported for the *Foxe3*^{-/-} mouse and retinal pigment epithelium (RPE) is abnormally separating the lens from retina and cornea.

Supplemental Table 1. *FOXE3* genetic variants in familial thoracic aortic aneurysms and dissection families.

Amino Acid Substitution	Nucleotide change	Family	MAF (%)^a	Conser vation^b	Predicted effect on function^c	Cscore
<i>Likely to be pathogenic</i>						
p.Gly137Asp	c.410G>A	MS300	0.0017	1	4/6	20.5
p.Asp153His	c.457G>C	TAA337	0.0008	1	5/6	17.25
p.Arg164Ser	c.490C>A	TAA141	0.0009	0.882	5/6	18.48
<i>Unknown significant</i>						
p.Asp156Asn	c.466G>A	TAA436	0.0293	1	6/6	32.0
<i>Unlikely to be pathogenic</i>						
p.Pro112Ser	c.334C>T	TAA086	0.0067	0	0/6	0.076
p.Pro202Leu	c.605C>T	MS2116	0.0098	0	0/6	12.28

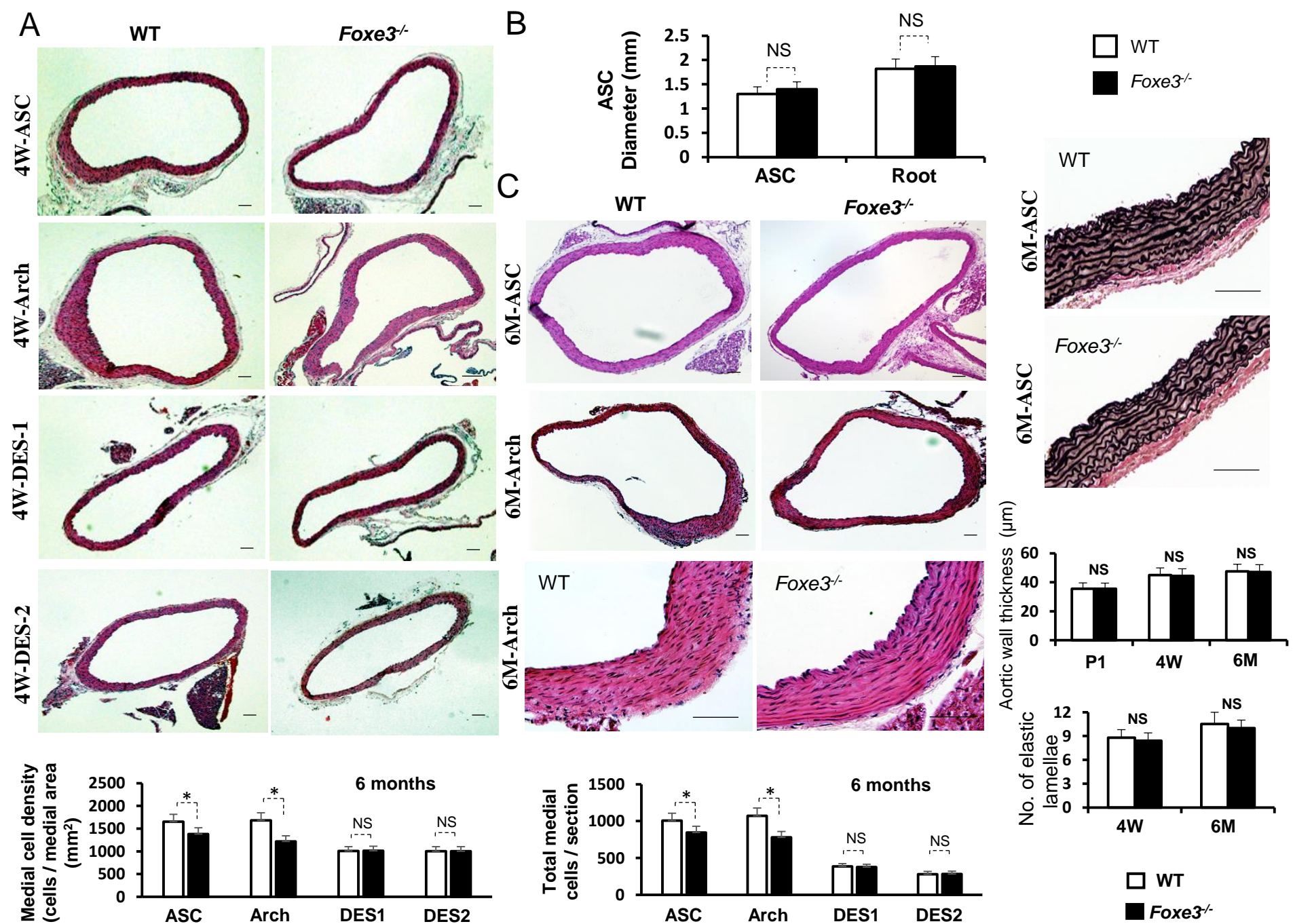
^a Minor allele frequencies in the Exome Aggregation Consortium (ExAC) database, <http://exac.broadinstitute.org/>

^b PhastCons conservation score

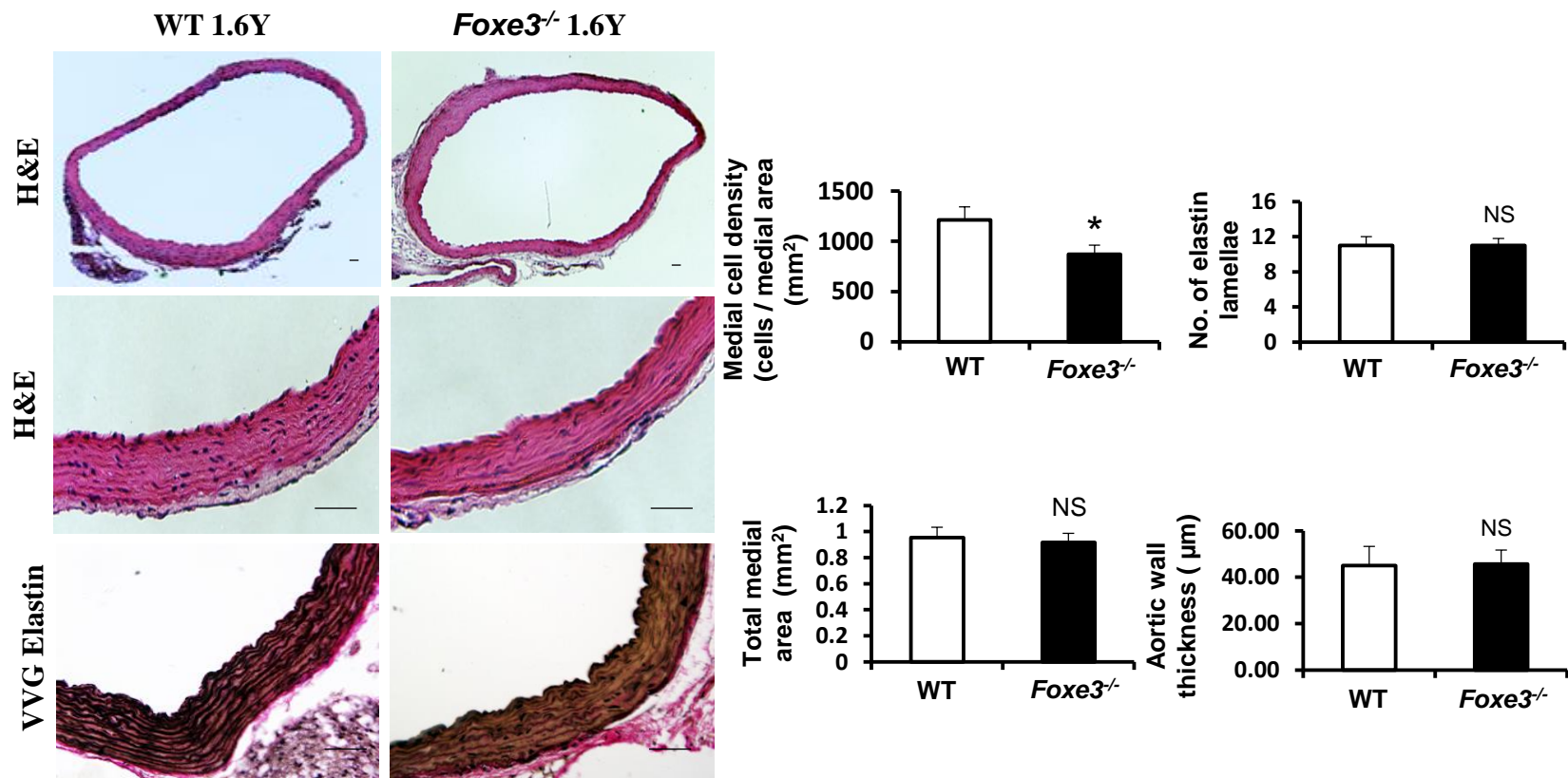
^c Predicted to be damaging in number out of 6 *in silico* prediction tools including: MutationTaster, Polyphen2_HDIV, Polyphen2_HVAR, SIFT, PROVEAN, and MutationAssessor.

Supplemental Table 2. Sequence of primers used in mouse PCR genotype analysis

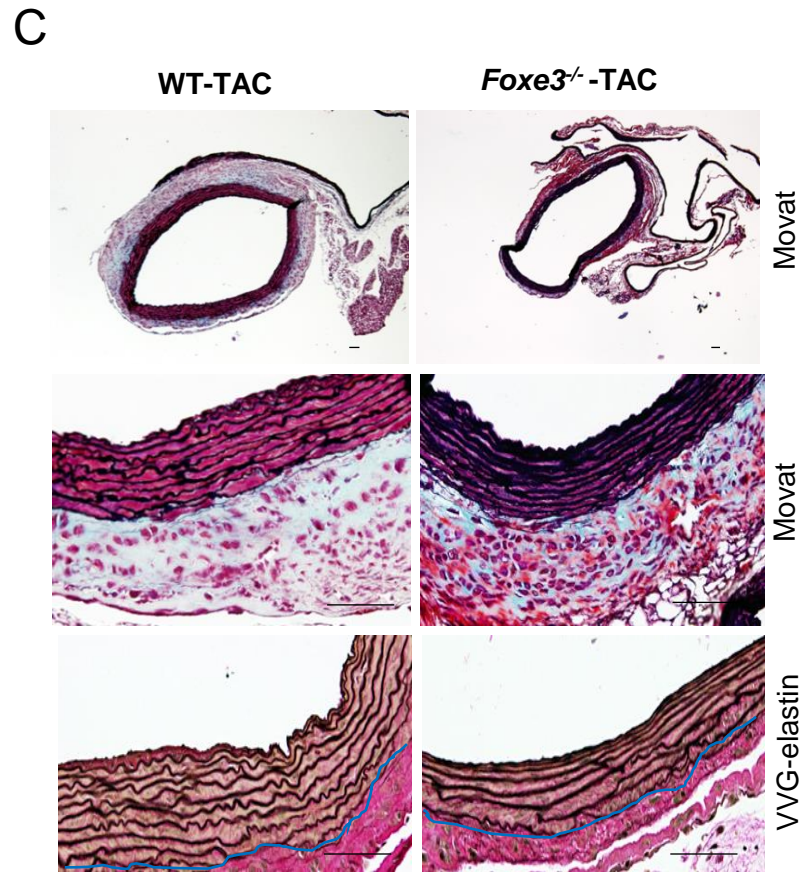
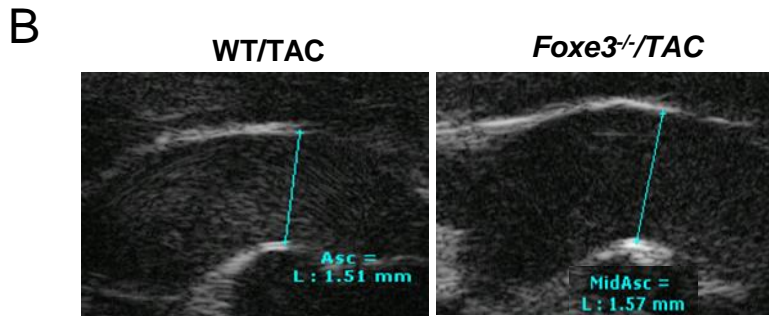
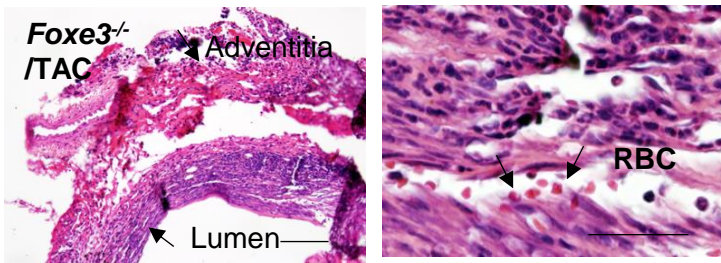
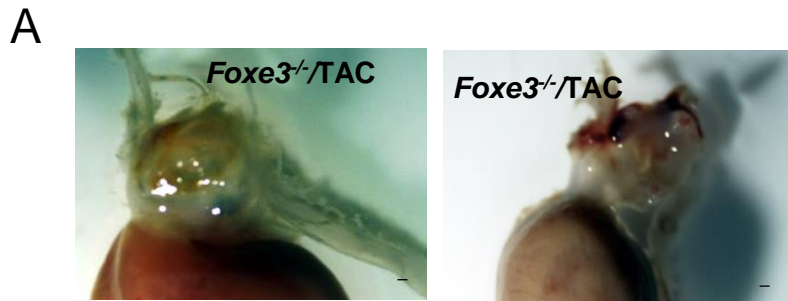
Gene	Primers	Primer sequence (5' to 3')	PCR Size
Foxe3 knockout genotype	Foxe3 forw	CGGGTACCGGGACTACTGATA	WT, 520bp
	Foxe3 rev	CTCGGACCTGCCCTCTAAT	
	Foxe3 forw	CGGGTACCGGGACTACTGATA	KO, 550bp
	Foxe3 NeoP	CTACCCGCTTCCATTGCTCA	
p53 knockout genotype	p53X6	AGCGTGGTGGTACCTTATGAGC	WT, 430bp
	P53X7	GGATGGTGGTATACTCAGAGCC	
	P53 neo	TCCTCGTGCTTTACGGTATC	KO, 600bp
	P53X7	GGATGGTGGTATACTCAGAGCC	



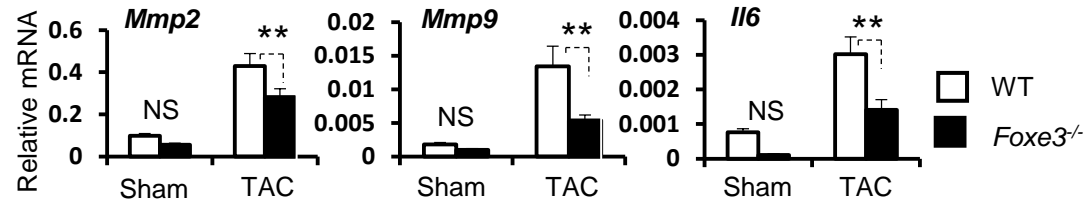
Supplemental Figure 1



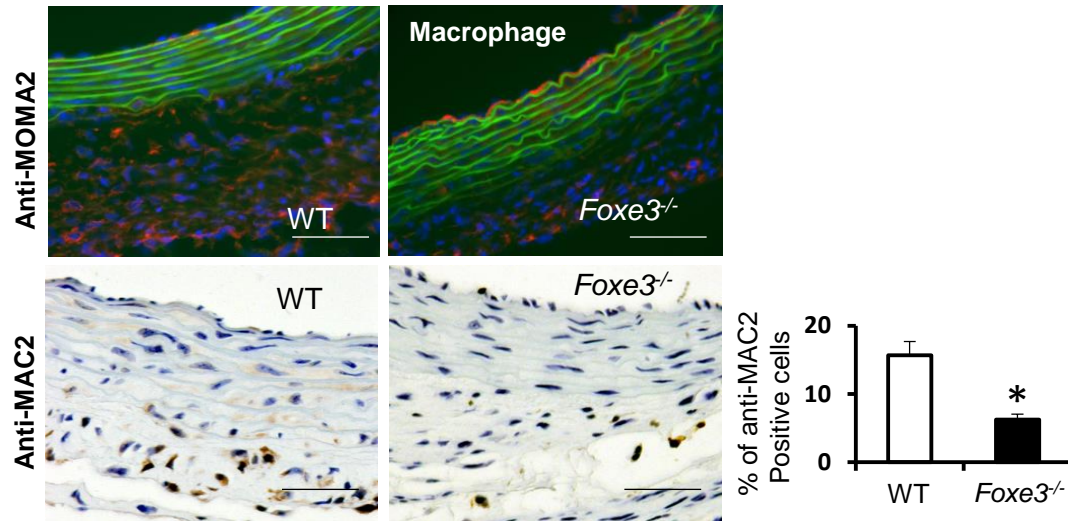
Supplemental Figure 2



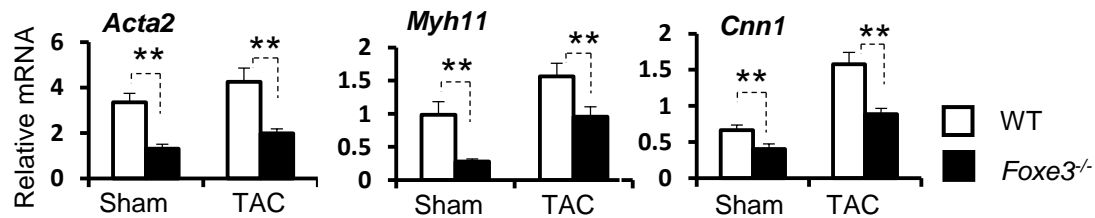
A

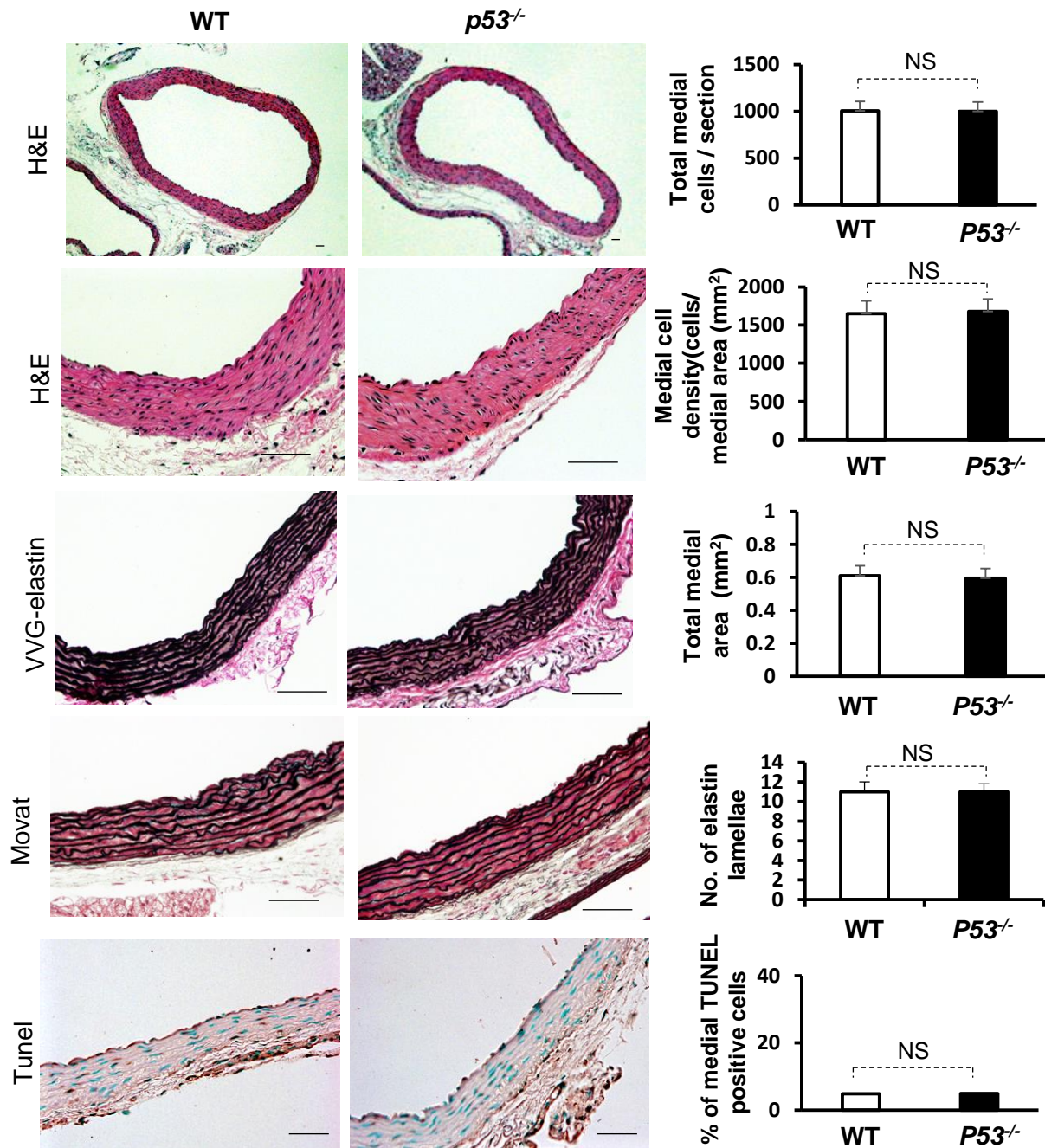


B

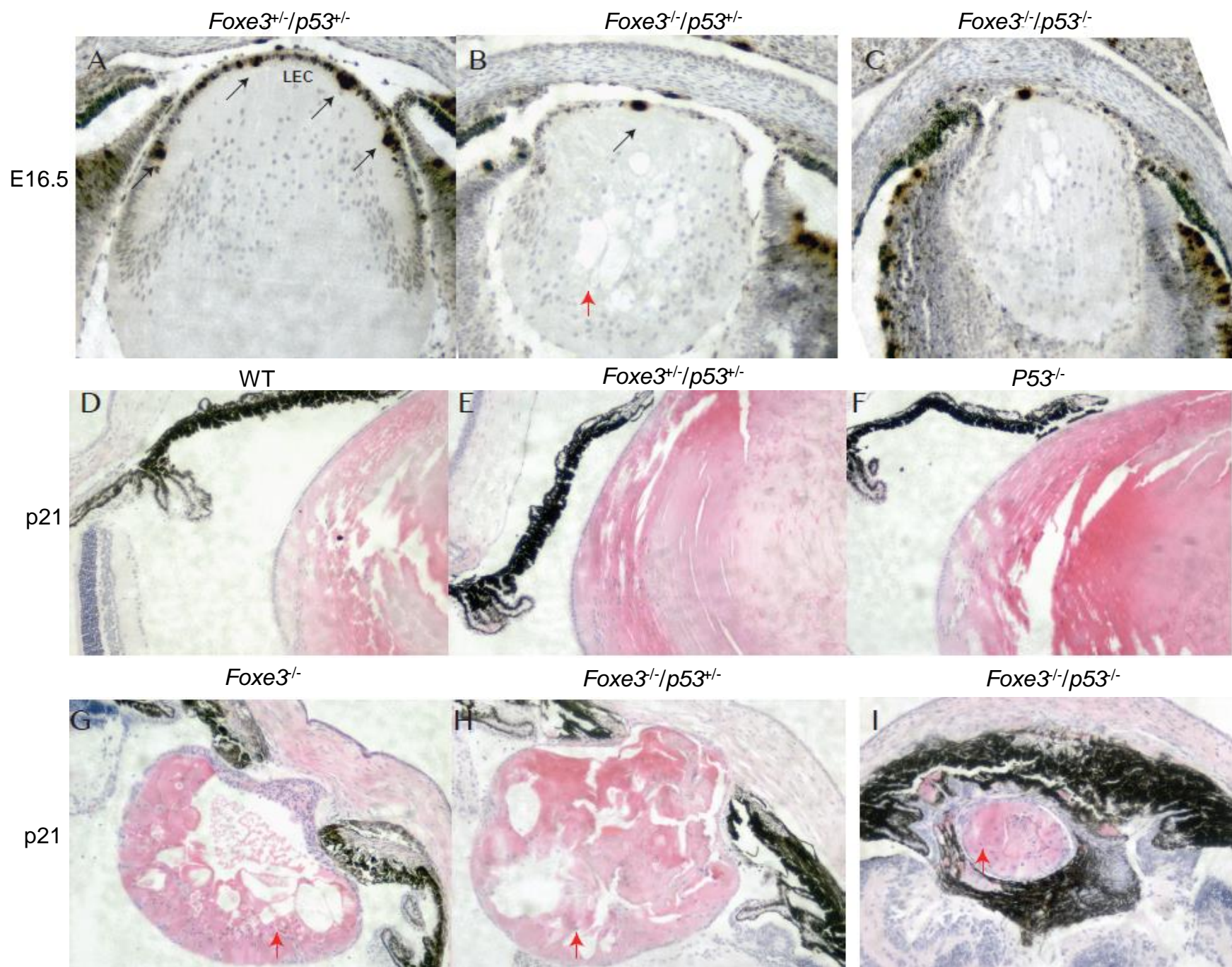


C





Supplemental Figure 5



Supplemental Figure 6

Supplemental data

Supplemental Acknowledgments for study group details.

Mutations in *FOXE3* Cause Familial Thoracic Aortic Aneurysms and Dissections

S.Q. Kuang¹, O. Medina-Martinez², D.C. Guo¹, L. Gong¹, E.S. Regalado¹, C.L. Reynolds³, C. Boileau⁴, G. Jondeau⁵, S.K. Prakash¹, C.S. Kwartler¹, L.Y. Zhu¹, A.M. Peters¹, X.Y. Duan¹, GenTAC Investigators, National Heart, Lung, and Blood Institute Go Exome Sequencing Project; M.J. Bamshad⁶, J. Shendure⁶, D.A. Nickerson⁶, R.L. Santos-Cortez⁷, X.R. Dong⁸, S.M. Leal⁷, M.W. Majesky⁸, E.C. Swindell⁹, M. Jamrich², D. M. Milewicz¹

The GenTAC investigators and their affiliations.

Williams Ravekes, M.D.

Harry C. Dietz, M.D., Ph.D.

Jennifer Habashi, M.D.

Johns Hopkins University, Baltimore, MD, USA

Dianna M. Milewicz, M.D. Ph.D.

Siddharth K. Prakash, M.D., Ph.D

University of Texas Health Science Center at Houston, Houston, Texas, USA

Scott A. LeMaire. M.D.

Shaine A. Morris, M.D.

Baylor College of Medicine, Houston, Texas, USA

Cheryl L Maslen, Ph.D.

Howard K. Song, M.D., Ph.D

G. Michael Silberbach, M.D.

Kathryn W. Holmes, M.D.

Oregon Health & Science University, Portland, OR, USA

Reed E. Pyeritz, M.D., Ph.D.

Joseph E. Bavaria M.D.

Karianna Milewski, M.D., Ph.D.

University of Pennsylvania, Philadelphia, PA, USA

Richard B. Devereux, M.D., Ph.D.

Jonathan W. Weinsaft, M.D.

Mary J. Roman, M.D.

Weill Medical College of Cornell University, New York, NY, USA

Ralph Shoet, M.D.

The Queen's Medical Center, Honolulu, HI, USA

Federico M. Asch, M.D.

MedStar Health Research Institute, Hyattsville, Maryland, USA

Kim A. Eagle, M.D.

University of Michigan, Ann Arbor, MI, USA

H. Eser Tolunay, Ph.D.

Patrice Desvigne-Nickens, M.D.

National Heart, Lung, and Blood Institute, NIH, Bethesda, MD, USA

Hung Tseng, PhD

National Institute of Arthritis, Musculoskeletal and Skin Diseases, NIH, Bethesda, MD, USA

Barbara L. Kroner, Ph.D.

RTI International, NC, USA